

Symmetries for a High Level Neural Decoder on the Toric Code

Thomas Wagner, Hermann Kampermann, Dagmar Bruß

Institute of Theoretical Physics III, Heinrich-Heine-Universität Düsseldorf,
Universitätsstraße 1, 40225 Düsseldorf, Germany

E-mail: thomas.wagner@uni-duesseldorf.de

November 26, 2021

Abstract. Surface codes are a promising method of quantum error correction and the basis of many proposed quantum computation implementations. However, their efficient decoding is still not fully explored. Recently, approaches based on machine learning techniques have been proposed by Torlai and Melko [20] as well as Varsamopoulos et al. [21]. In these approaches, a so called high level decoder is used to post-correct an underlying decoder by correcting logical errors. A significant problem is that these methods require large amounts of training data even for relatively small code distances. The above-mentioned methods were tested on the rotated surface code which encodes one logical qubit. Here, we show that they are viable even for the toric surface code which encodes two logical qubits. Furthermore, we explain how symmetries of the toric code can be exploited to reduce the amount of training data that is required to obtain good decoding results. Finally, we compare different underlying decoders and show that the accuracy of high level decoding noticeably depends on the quality of the underlying decoder in the realistic case of imperfect training.

1. Introduction

A great challenge in the practical realization of quantum computing is the presence of noise which spoils accurate control of physical systems. The effect of such noise can be mitigated by using quantum error correction. The physical state of a system is encoded into the logical state of a quantum code. Then, computations can be performed on the logical level of the code. As coding introduces redundancy in the data, many errors can be detected and corrected by a decoder. According to the threshold theorem [16, 1], quantum error correction allows us to perform quantum computations with arbitrary accuracy as long as all single component error rates are below a certain threshold. A promising approach to quantum error correction is the use of topological quantum codes. The surface code by Bravyi and Kitaev [3][15] possesses a high threshold error rate [19] above some existing experimental error rates [5]. Furthermore, it has the advantage of only requiring nearest neighbour interactions. However, a problem in the practical realization of surface codes is the need for decoders that are both fast and accurate. Fast decoding is crucial because the decoding procedure should be shorter than the coherence time of the qubits, which can be of order $1 \mu s$. [19].

Several different decoders based on various approximations have been proposed [2, 6, 11]. These decoders are generally based on the assumption of independent Pauli noise, and it is not always clear how they can be adapted to experimental noise. Recently, there has been an increasing interest in decoders based on machine learning techniques. These decoders are trained on a set of known errors and then learn to generalize to new errors. This allows for adaptability to experimental noise. The first such decoder was developed by Torlai and Melko [20] and is based on stochastic neural networks. It was introduced for the toric surface code with only phase-flip errors, but the techniques are generalizable to all stabilizer codes. Another approach, called high level decoder, based on more conventional feed forward neural networks was proposed by Varsamopoulos et al. [21][22] and further explored by Chamberland and Ronagh [4]. This approach was implemented on the so called rotated surface code, which encodes one qubit, for different noise models including circuit noise. In [4] it is concluded that, once the decoder is trained, the actual decoding procedure of feed forward neural network based decoders is fast enough to be scalable to larger codes. A high performance computing platform is still required. Furthermore, Maskara et al. [17] demonstrated that the method is applicable to different architectures, such as color codes and toric codes on triangular lattices, and various noise models. However, it is also pointed out in [4] that the training of decoders becomes increasingly difficult for larger codes. So far, the method is only applicable to small codes with a distance less than seven. The amount of training data needed to train the networks for larger codes is infeasible. One way to approach this problem are decoders based on local regions of the code [23][18]. This technique is inspired by the renormalization group decoder [6].

To supplement these approaches, in this paper, it will be shown how symmetries of the toric code can be explicitly incorporated into the training of (feed forward) neural

network based decoders. This reduces the amount of training data needed substantially and improves the quality of training. Our approach will be demonstrated for the high level decoder developed by Varsamopoulos et al. [21][22], but it is applicable to general machine learning based decoders. This decoder was chosen as an example because it is a relatively simple but still effective machine learning based decoder, and because it was well explored in previous work [21, 22, 4]. Furthermore, it is demonstrated that it is possible to train good high level decoders for the toric code encoding two logical qubits. Previous literature considered the rotated surface code which only encodes one logical qubit. The main difference here is in the number of possible logical errors, which is larger by a factor of four for the toric code.

This paper is structured as follows. First, a short introduction about the toric code is given, and standard decoders for the code are reviewed. Next, the high level decoder scheme [21] is described. Then, it will be explained how symmetries of the toric code can be exploited to improve this decoder. Finally, some numerical results will be presented which demonstrate the increase in performance provided by the inclusion of symmetries.

2. The Toric Code and Noise Model

Although the core ideas are applicable to a wider range of codes, the techniques in this paper will be constructed for the toric code developed by Bravyi and Kitaev [3][15]. We give a short description of this code here. (See [8] for an in depth review.) The toric code is a stabilizer code that is defined on an $L \times L$ square lattice embedded on a torus. The lattice consists of vertices, edges and faces. Four edges are connected to each vertex, and each face is surrounded by four edges (Figure 1). Each edge of the lattice is associated with a physical qubit of the code. In the following we denote the Pauli X / Pauli Z operator acting on the qubit associated with edge e of the lattice by X_e / Z_e . The vertices and faces of the lattice are associated with stabilizer operators. Each vertex v represents a *star* operator:

$$X_v = \prod_{e \in \partial^0 v} X_e \quad (1)$$

where $\partial^0 v$ is the coboundary of v , i.e. the set of four edges connected to v . Similarly, each face f represents a *plaquette* operator:

$$Z_f = \prod_{e \in \partial_1 f} Z_e \quad (2)$$

where $\partial_1 f$ is the boundary of f , i.e. the set of four edges adjacent to f . The stabilizer group S consists of all possible products of the stabilizer operators above. The toric code is then defined as the common eigenspace with eigenvalue +1 of all operators in S . The code encodes two logical qubits, because S is generated by $2L^2 - 2$ independent generators and there are $2L^2$ physical qubits in the code. Pauli operators acting on the code can be represented as chains of edges on the lattice, by marking which qubits are affected by a Pauli Z or Pauli X operator. There are 16 logical operators, corresponding to the two qubit Pauli group, that map between the codewords of the toric code. These

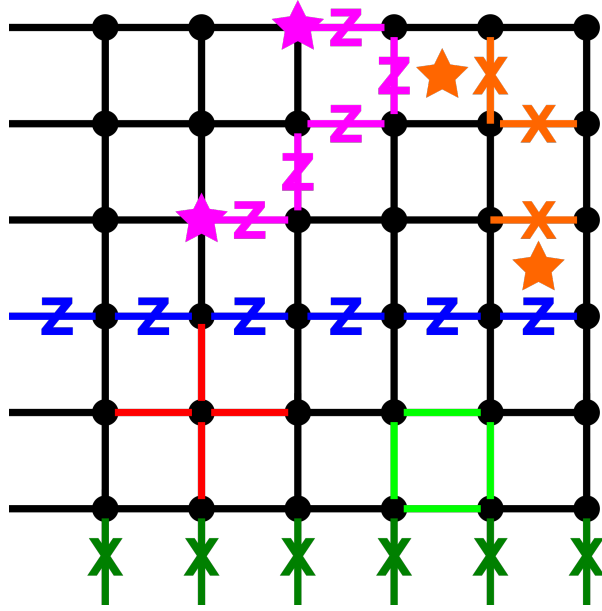


Figure 1: Representation of the 6×6 toric code. Note that the boundary of the lattice is periodic. The edges leaving at the left border wrap back around to the right and the edges leaving at the bottom wrap back around to the top. Shown are examples of different error chains. In blue and dark green, logical Z_1 and X_1 operators are shown. In pink, a detectable Z error chain is shown. Its syndrome is marked by the pink stars on the corresponding vertices. Similarly, a detectable X error chain is shown in orange, and its syndrome is marked by the orange stars on the corresponding faces. In red, a star operator is shown, and in bright green a plaquette operator is shown.

operators correspond to loops on the lattice, as illustrated in Figure 1. They will be denoted with a subscript to indicate which logical qubit they act on, e.g. the logical Z_1 operator is the logical Z operator that acts on the first logical qubit.

If no errors affect the code, the measurement of each stabilizer operator will result in a $+1$ outcome. If an error e affects the code, it might anti-commute with some stabilizer operators. The stabilizers that anti-commute with the error will flip their measurement outcome to -1 . These are called *detections*, and together they form the *syndrome* of the error. As an example, in the case of a Z error chain, the detections are located at the vertices at the end points of the error chain on the lattice. For these errors the task of a decoder is to propose, based on the syndrome, a recovery chain r that eliminates the error. The recovery was successful if the product of the error and the recovery lies in the stabilizer group. As an example, for Z errors this means that the error and the recovery form the boundary of a region on the lattice. This also implies that all recoveries that only differ by stabilizer operators are logically equivalent. It is therefore not necessary to deduce the exact error that occurred, but only its equivalence class up to stabilizer applications.

We will consider the toric code subject to local depolarizing noise. In this model, errors occur independently on each physical qubit. Each physical qubit is either unaffected by noise with probability $1 - q$ or replaced by the completely mixed state with probability q . The action on the density operator ρ of one qubit is therefore expressed by the quantum channel:

$$\rho \mapsto (1 - q)\rho + q\frac{I}{2} = (1 - \frac{3}{4}q)\rho + \frac{q}{4}(X\rho X + Y\rho Y + Z\rho Z) \quad (3)$$

Thus, the channel can be simulated by leaving each qubit untouched with probability $1 - p$, where $p = \frac{3}{4}q$, or applying exactly one of the three Pauli operators each with probability $\frac{p}{3}$. The error rate p will also be referred to as *depolarizing noise parameter*. Note that the stabilizer measurements are assumed to be perfect.

3. Simple Decoders for the Toric Code

Here, we will shortly describe two simple ways of decoding the toric code.

The first is *minimum weight perfect matching* (MWPM) based on Edmonds Blossom algorithm [7]. This decoder will be used as a benchmark throughout this paper. Here, Z and X errors are decoded independently. The Z / X recovery is found by proposing the shortest chain that matches the syndrom of the vertices / faces. This corresponds to finding the lowest weight error matching the syndrom, i.e. the error acting on as few physical qubits as possible. In our paper an implementation based on the *NetworkX* python package [10] is used. There are two problems with MWPM decoding. The first is that because Z and X errors are decoded independently, Y errors can lead to incorrect decoding because they introduce correlations between X and Z errors. Essentially, a Y error is counted as two separate errors which is only correct if X and Z errors are independent. In the depolarizing noise model this assumption is not correct. An example of this problem can be found in [6]. The second problem is that MWPM does not account properly for the effect of degeneracy. All errors that only differ by a stabilizer operator are logically equivalent. Therefore, it can happen that the most likely class of equivalent errors does not contain the most likely (shortest) error. This leads to suboptimal decoding. An example can again be found in [6]. The runtime of (unoptimized) MWPM scales as $\mathcal{O}(L^6)$ [6], which is already a problem for larger codes.

Therefore, it will be useful to introduce a simpler decoder. This *trivial decoder* is designed to return a recovery as fast as possible. First, we enumerate the stabilizer operators in some way, say from top left to bottom right in the lattice picture. The trivial decoder then works by matching the detections in a syndrome iteratively according to the above enumeration, using the shortest chain for each matching. This means the first detection is connected with the second, the third with the fourth and so on. Because the measurements are assumed to be perfect the total number of detections will always be even, so no detections are left unmatched. Because the number of expected detections increases quadratically in L , the runtime of this algorithm will also be quadratic in L .

The recovery proposed by this decoder is very inaccurate, but it will be useful as an initial decoding after which we apply a so called *high level decoder* (HLD).

4. High Level Neural Decoder

In [21] it was shown how decoding can be approached as a classification problem, which is standard in machine learning. Given a syndrom on the toric code, first some standard decoder is used which proposes a recovery chain that matches the measured syndrom. This will be referred to as the *underlying decoder*. Because the proposed recovery matches the syndrom, the product of the error and the recovery will form a logical operator. The classification task is then to predict the most likely logical operator based on the initial syndrom that was measured. Then, an additional recovery corresponding to the predicted logical operator can be applied. This essentially constitutes a post-correction of the underlying decoder. The basic problem is to correctly classify input vectors, corresponding to syndroms, into different classes, corresponding to logical operators. This decoding scheme is called a *high level decoder* (HLD). In [21] a surface code which encodes one logical qubit, called the rotated surface code, was considered. Therefore there were 4 possible logical errors, corresponding to a classification problem with 4 classes. Here we will consider the toric code, which encodes two qubits. Therefore the classification problem has 16 classes, corresponding to the two qubit Pauli group. The decoding process is illustrated schematically in Figure 2, using MWPM as the underlying decoder.

The classification task outlined above is approached with a simple and widely used machine learning model known as *feed forward neural network* (FFNN). An FFNN consists of several layers of real-valued units. The first layer corresponds to the input vector, and the last layer has one unit for each possible class label. Between them are several hidden layers. Each hidden layer applies a transformation of the form $\mathbf{y} = g(W\mathbf{x} + \mathbf{b})$ to the values of the previous layer, where the matrix W and the vector \mathbf{b} are free parameters that will be learned during training. They are called the weights and biases of the layer. The weights and biases of all layers together form the parameter vector $\boldsymbol{\theta}$ of the network. The function g is called the activation function. In this work it is chosen to be the rectified linear unit:

$$g(x) = \max(0, x) \tag{4}$$

applied elementwise to the vector. This is a standard choice in machine learning, for example suggested in [9]. The output layer instead uses the softmax activation function:

$$\text{softmax}(\mathbf{x})_i = \frac{\exp(x_i)}{\sum_j \exp(x_j)} \tag{5}$$

which is necessary for classification tasks. The parameters $\boldsymbol{\theta}$ of the model are found by considering a training set $T = \{(e, \ell)\}$ of errors with known logical errors, generated according to the depolarizing noise model. This training set defines a cross-entropy loss

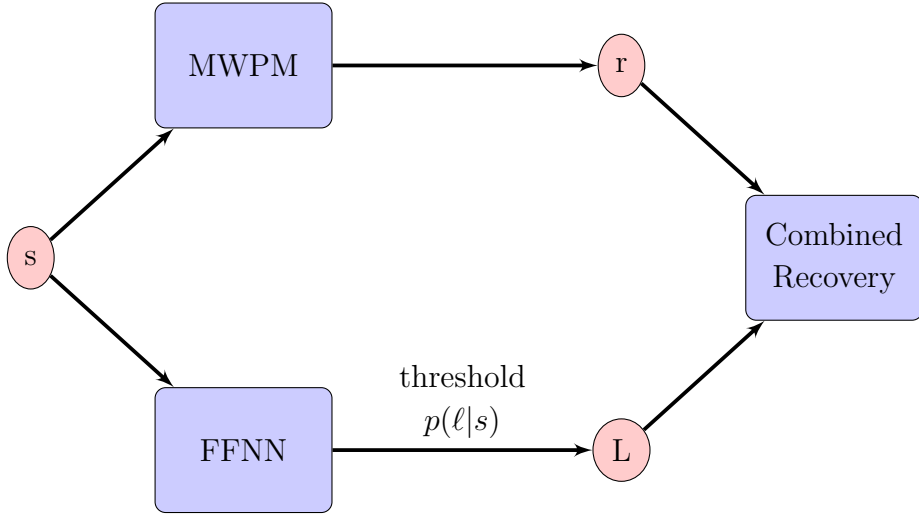


Figure 2: The decoding process of the high level decoder. A syndrome s is decoded by MWPM to obtain a physical recovery r , and by an FFNN to obtain the logical error ℓ of MWPM. The logical error is applied as post-correction to the MWPM decoding to obtain a combined recovery.

function:

$$E(\theta) = \sum_{(e,\ell) \in T} \ln(y_\ell(\mathbf{x}; \theta)) \quad (6)$$

where y_ℓ is the component of the output layer corresponding to the logical error ℓ . This loss function can be further modified by adding a *weight decay* term $\lambda \|\theta\|_2$ for some positive λ . This can help against overfitting issues by keeping the network parameters smaller [9]. The parameters θ are found by minimizing this loss function with the adaptive moment estimation algorithm [14], which is a variant of stochastic gradient descent. Before the first iteration of stochastic gradient descent the parameters are initialized randomly from a normal distribution. After the training, the model can be evaluated on test sets that were generated independently from the training set. All these methods were implemented with the Shark machine learning library [12].

The model has a number of hyperparameters that need to be chosen in advance. These are: The number n_{it} of iterations of stochastic gradient descent, the learning rate η used in stochastic gradient descent, the number n_h of hidden layers, the numbers of units l_i in the i 'th hidden layer, the strength λ of weight decay regularization, and the width of the distribution used for initialization. These parameters need to be chosen sensibly according to some heuristic, usually with some trial and error involved.

It should be stressed that the accuracy of the model strongly depends on the quality and size of the training set. If the training set is too small the model will be unable to learn the real distribution of logical errors. This usually manifests in overfitting, i.e. the accuracy on the training set is good but the accuracy on the test sets is bad. This is especially problematic for larger code distances, where a large amount of different syndroms should be represented in the training data. Finally, it should be noted that

the best performance is reached if the training set is generated at the same physical error rate as the test set the model should be used for [22]. However, the models can still generalize well to different error rates.

5. Symmetries of the Toric Code

In order to learn the correct conditional distributions of logical errors given syndromes, the model needs to have a large selection of syndromes available in the training data. Preferably each syndrome should appear multiple times to make the prediction of the most likely logical error more accurate. For a 7×7 surface code the input space consists of 2^{98} different possible syndromes so the amount of training data needed is already very large. Here, we will describe how symmetries of the code can be explicitly incorporated into the training of decoders in order to reduce the effective size of the input space. This reduces the amount of training data that is needed or, alternatively, allows for better results with the same amount of training data.

There are several symmetries on the toric code, including exchange, translation and mirror symmetry. Here we will focus mainly on translation and exchange symmetry. Translation symmetry means that the code is invariant under a translation of the vertices, edges and plaquettes, taking into account the periodic boundary conditions. Exchange symmetry means that the toric code is invariant under an exchange of the toroidal and poloidal direction on the torus, provided one choses a lattice with the same number of edges in both directions. The exchange does however correspond to a relabeling of the logical operators. In the lattice view of the code, which is shown in Figure 1, this corresponds to an anti-transposition of the lattice. Note that if one considers surface codes that include holes or different boundary conditions, the symmetries mentioned above might be broken. Different symmetries will be applicable depending on the exact layout of the surface code.

5.1. Including Translation Symmetry by using Centered Data

We start by describing the concepts using the example of translation invariance. Later it will be described how to incorporate exchange invariance and other symmetries.

It is expected that two syndromes that only differ by a translation should have the same logical error. (Some care has to be taken here because it is implicitly assumed that the underlying decoder respects the translation invariance, more on this below.) With infinite training data an HLD should learn this invariance by "brute-force". As the training data is limited in practice it is better to explicitly include this invariance. Therefore, one unique representant of each translation class of syndromes should be chosen. The training data is then pre-processed by mapping each syndrome to its translation representant. Of course, when decoding the syndromes also need to be pre-processed. This costs some additional computational resources. The pre-processing guarantees that the HLD includes the translation invariance, and thus reduces the

amount of different syndromes the decoder needs to learn.

Explicitly, a pre-processing function can be constructed by using a lexicographic ordering of the syndromes. Enumerating the vertices and plaquettes in some way, say from top left to bottom right on the lattice, syndromes can be represented as binary vectors. The i 'th entry of such a vector is 1 if the i 'th vertex has a detection, and 0 otherwise. Analogously one defines a vector for the plaquette detections. The vector representing the plaquette results is appended to the vector representing the vertex results. We can then define a total ordering on syndromes as follows:

Definition 1 (Lexicographic ordering of syndromes) *For two syndromes s_1, s_2 represented as binary vectors, define $s_1 < s_2$ if the first non-zero entry of $s_1 - s_2$ is 1.*

In other words, $s_1 < s_2$ if the first non-zero entry of s_1 comes "before" the first non-zero entry of s_2 . The subtraction in the definition is NOT meant mod 2. Note that if $s_1 - s_2 = 0$, so no non-zero entries exist in $s_1 - s_2$, then $s_1 = s_2$.

Using this ordering, a "centering" algorithm that maps a syndrome to a well defined translation representant can be defined as follows:

Algorithm 1 (Centering) *Given a syndrome s , first compute all possible ways to translate it such that a vertex detection is in the upper left corner (the first vertex) of the code. If the syndrome has n vertex detections, there are n possible ways to do this. If there are no vertex detections, instead compute the ways to translate a plaquette detection into the upper left corner. Then, compare all the translated syndromes according to the ordering in definition 1 and choose the minimal one according to this ordering. This will result in a uniquely defined representant of each translation class.*

Algorithm 1: Centering algorithm used to obtain a unique translation representant for each syndrome.

Input : Syndrome s as binary vector of length $2L^2$
Output: Translation representant s_c of the syndrome as binary vector
 $T \leftarrow \{\text{Translation}(s) \mid \text{first element of Translation}(s) \text{ is } 1\}$
if T not empty:
 | $s_c \leftarrow \min(T)$
 | return s_c
else:
 | $T \leftarrow \{\text{Translation}(s) \mid \text{element } L^2 + 1 \text{ of Translation}(s) \text{ is } 1\}$
 | **if** T not empty:
 | $s_c \leftarrow \min(T)$
 | return s_c
 | **else:**
 | return empty syndrome

Of course, this algorithm straightforwardly generalizes to any other possible symmetry. In order to find a unique representant, one first computes all possible

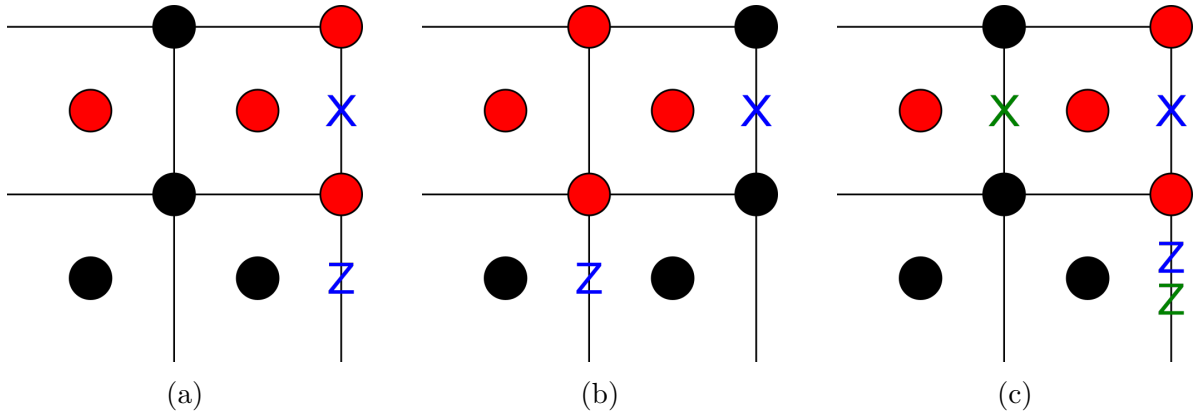


Figure 3: The red dots show two syndromes (a) and (b) on a 2×2 toric code that differ by a one step translation in the horizontal direction. In blue, the recoveries proposed by MWPM decoding are shown. (c) shows the recovery proposed by normal MWPM in blue. The recovery one obtains by applying MWPM to the centered syndrome (b) and then translating back is shown in green. Notice that the proposed recoveries differ by a logical X operator.

representants and then chooses the minimal one according to the lexicographic ordering. Finally, it should be noted that the underlying decoder does not necessarily respect the translation invariance of the code. Given two syndromes that only differ by a translation, it is possible that the underlying decoder returns two recoveries that do not only differ by a translation, but by a translation and a logical operator. A simple example of this problem on a 2×2 code for MWPM is shown in Figure 3. Therefore it is important that all syndromes are centered before applying the underlying decoder to them. The recovery proposed by the underlying decoder then needs to be translated back to match the original syndrome. In this way it is guaranteed that the underlying decoder is compatible with translation invariance. The same principle applies to all other invariances one might want to incorporate.

5.2. Including Exchange Invariance by using Aligned Data

In addition to translation invariance, which has the largest effect, further symmetries can be included. Here, the case of exchange invariance is considered. The basic principle for pre-processing is the same as for translation invariance: One first computes the two possible anti-transpositions of the syndrome, then chooses the one that is minimal according to the lexicographic ordering (definition 1). Again, pre-processing should take place before applying the underlying decoder, and the proposed recoveries need to be anti-transposed back to match the original syndrome. Furthermore, as mentioned above, an anti-transposition corresponds to a relabeling of the logical operators. The logical Z_1 and Z_2 operators are exchanged with each other, and the logical X_1 and X_2 operators are exchanged with each other. Therefore, here, the class labels of the training data need to be adapted if there were anti-transpositions in the pre-processing.

Similarly, the logical error proposed by the high level decoder during online decoding needs to be corrected for the effect of anti-transpositions. Note that no such correction was necessary in the case of translation invariance as the logical operators are invariant under translations.

In the following, we will use s^t to denote the anti-transposition representant of a syndrome s . When combining both translation and exchange invariance, the naive approach is to first compute the representant of the anti-transposition class of a syndrome, and then center this representant. This approach does not work, as illustrated with an example on the 3×3 toric code in Figure 4. Different translations of the same syndrome will result in different representants. Therefore, a slightly more complicated algorithm has to be used. This algorithm will be called "alignment" algorithm and is described in the following:

Algorithm 2 (Alignment) *Given a syndrome s , it is first centered to obtain s_c . Then, the anti-transposition representant s_c^t of s_c is computed and also centered to obtain $(s_c^t)_c$. The two syndromes s_c and $(s_c^t)_c$ are compared and the minimal of the two is chosen. This pre-processing will map syndromes that differ only by translations and anti-transpositions to the same syndrome.*

Algorithm 2: Alignment algorithm used to obtain a unique representant under combined translations and anti-transpositions for each syndrome.

Input : Syndrome s as binary vector of length $2L^2$

Output: Representant s_a of the syndrome under combined translations and anti-transpositions as binary vector

$s_c \leftarrow \text{Center}(s)$

$s_c^t \leftarrow \text{Anti-transposition Representant}(s)$

$(s_c^t)_c \leftarrow \text{Center}(s_c^t)$

return $\min(s_c, (s_c^t)_c)$

Again, the underlying decoder might not be compatible with the alignment by default. To rectify this issue, the same strategy as above is employed. Instead of decoding a syndrome s directly, the aligned syndrome s_a is decoded. All transformations (both translations and anti-transpositions) applied to s in order to obtain s_a are tracked. The recovery proposed by the underlying decoder is then transformed back to match the original syndrome s .

5.3. Estimate Scaling of the Centering Algorithm

To get an idea of whether the centering algorithm is applicable to larger codes, an estimate of its runtime scaling with the code distance is given here. As the alignment algorithm mainly consists of multiple applications of centering, the scaling will be the same. The centering algorithm uses a list with one entry for each detection in a syndrome. For the case of large L and small error rates, the average number of detections is assumed to scale with L^2 . Finding the minimum of a list of length n can be done in

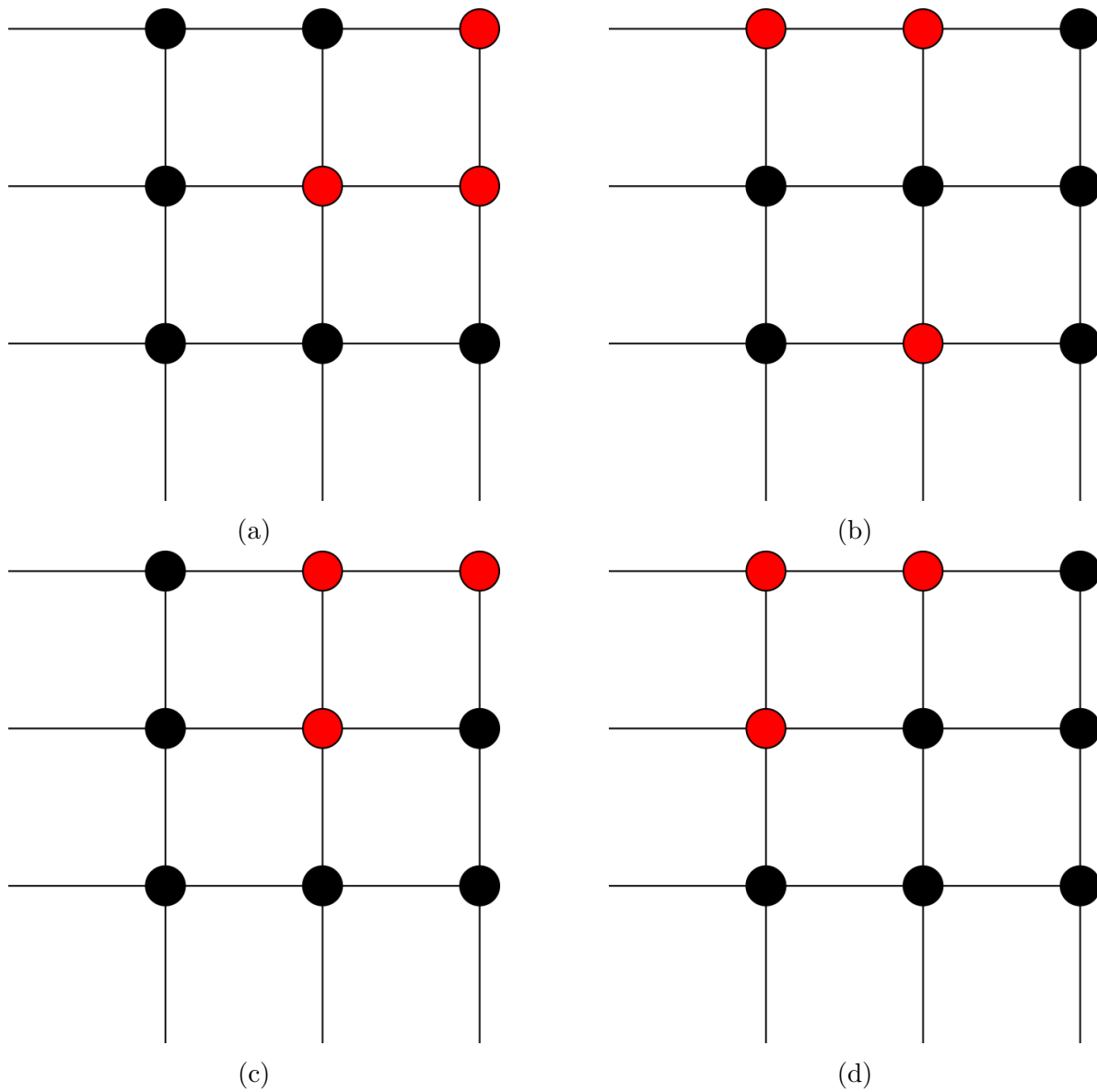


Figure 4: Example of why the naive approach to combining transposition and translation invariance does not work. The syndromes (a) and (b) differ by a translation. Computing the anti-transposition representant of (a) one obtains syndrome (c) and then centering it one obtains syndrome (d). However the transposition representant of syndrome (b) is syndrome (b) itself, and centering it one obtains again syndrome (b).

$n - 1$ comparisons. A single comparison according to the lexicographic ordering scales with L^2 in the worst case, because a syndrome vector has a length of $2 * L^2$. This would give a scaling of $\mathcal{O}(L^4)$. We assume that the distribution of detections in the different translations of the syndrome is approximately random. It is thus likely that a difference between two syndromes can already be found in the first few entries. Therefore, the comparison will terminate after an average number of steps that is independent of L^2 , although this average number of steps does depend on the error rate p and will be larger for small error rates where only few detections are present. The average runtime is therefore estimated to be proportional to $\mathcal{O}(L^2)$. As a point of reference, MWPM decoding has a scaling of $\mathcal{O}(L^6)$. The trivial decoder described in section 3 matches the detections iteratively, so it scales linearly in the number of detections and thus quadratically in L . Therefore, the average case scaling of centering matches the scaling of the trivial decoder. There is hope that the additional overhead during decoding that arises from the inclusion of symmetries is manageable.

6. Numerical Results

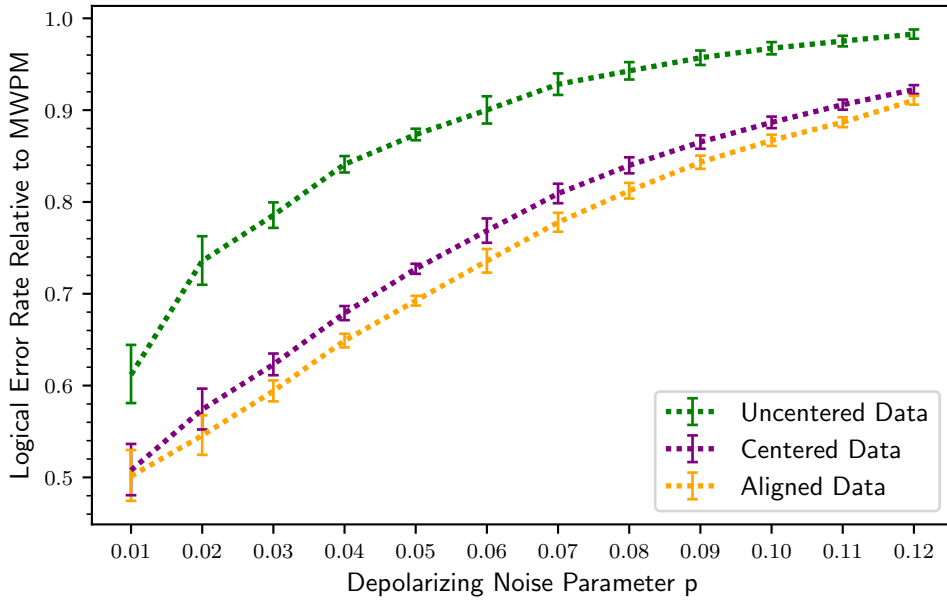
The algorithms described above were tested on the 3×3 , 5×5 and 7×7 toric code. Different FFNNs were trained for use in high level decoders. Networks were trained incorporating either no symmetries (uncentered data), only translation symmetry (centered data) or both translation and exchange symmetry (aligned data). As a shorthand, networks trained with uncentered / centered / aligned data are sometimes referred to as uncentered / centered / aligned networks. For simplicity, the training data was always generated at noise parameter $p = 0.01$. The weights of the networks were always initialized from a normal distribution with width 0.01. For stochastic gradient descent, a batch size of 1000 was used. No weight decay was employed unless otherwise specified. Following [21], two hidden layers with decreasing number of units were used. The input layer had the size $2L^2$, corresponding to the size of a syndrome, and the output layer had the size 16, corresponding to the 16 possible logical errors. Note that this is in contrast to the decoders tested in [21, 4, 23] on the rotated surface code, where only 4 logical errors were possible. Therefore this work also shows that the high level decoding scheme can be applied to surface codes with a larger number of qubits. The trained decoders were tested for depolarizing noise parameters $p = 0.01$ to $p = 0.18$ in steps of 0.01. Unless otherwise specified a test set of size 10^6 was used for each noise parameter. The error bars in the plots represent 95% confidence intervals. They were obtained by approximating the logarithm of the ratio of binomial proportions by a normal distribution as described in [13].

We start by considering HLDs on the 5×5 toric code using MWPM as the underlying decoder. Here, using a training set of size $9 * 10^6$ was sufficient to obtain significant improvements over standard MWPM even when not accounting for symmetries. However, when accounting for symmetries, about another 20% relative improvement could be obtained. The error rates with and without symmetries, relative

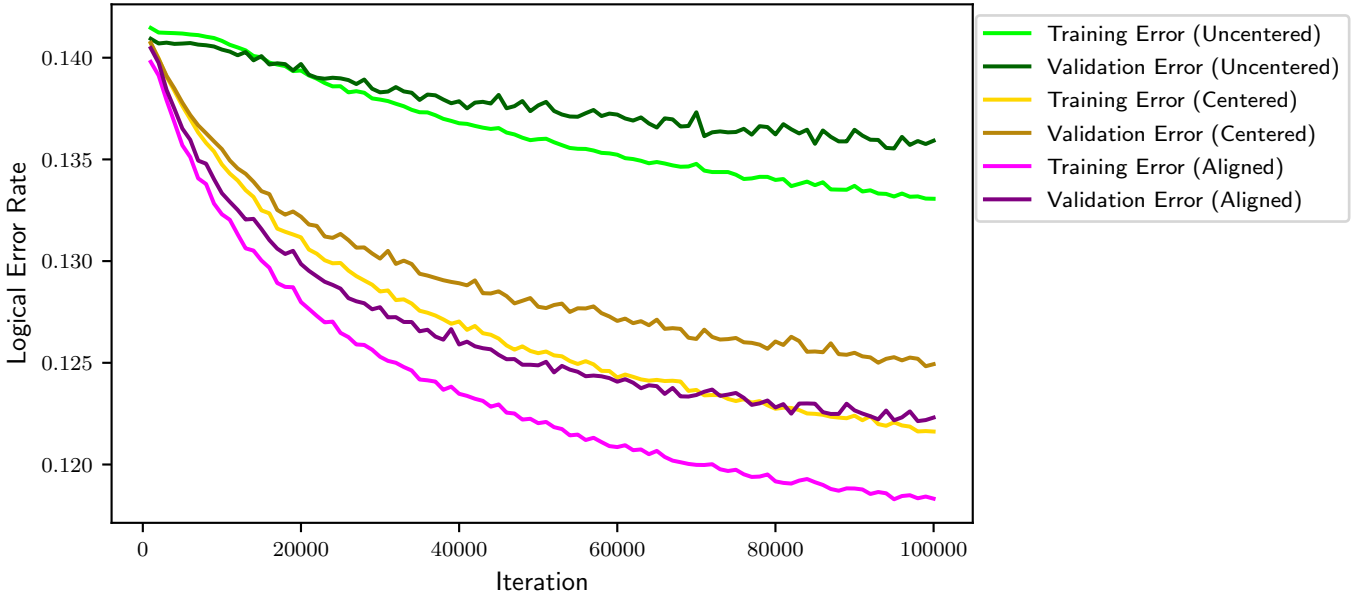
to MWPM, are compared in Figure 5a. Shown is the relative logical error rate $p_{\text{decoder}}/p_{\text{MWPM}}$ for high level decoders trained on the same dataset, but either not accounting for symmetries (uncentered), accounting only for translation invariance (centered) or accounting for both translation and exchange invariance (aligned). The logical error rate is shown for different depolarizing noise parameters. It can be seen that using translation invariance allows for a large improvement over standard MWPM, and further accounting for exchange invariance leads to another small improvement. It is indeed expected that translation invariance leads to larger improvements than exchange invariance. The reasoning is that the translation class of a syndrome contains up to L^2 elements, while the anti-transposition class of a syndrome contains only up to 2 elements. The difference between aligned and centered data becomes less pronounced for smaller error rates, as the decoder is more accurate for small syndromes by default. Considering the training of the decoders, one observes that including symmetries leads to improvements in both validation and training error. (Figure 5b) Therefore the pre-processing actually allows for a more accurate fit even to the training data, i.e. the data was presented in a form more suitable to the model.

To investigate by how much we can reduce of the size of the training set, decoders with uncentered or aligned data were trained with training sets of size $4.5 * 10^6$, $2.7 * 10^6$ and $1.8 * 10^6$. The training for the smallest data size is compared in Figure 6. No improvement over MWPM could be reached without the use of symmetries. Aligning the data on the other hand does allow for improvements. Again, both validation and training error are improved. However, the validation error does increase again in later iterations of training. Therefore we expect that it is not possible to use even less training data and still obtain good results. The aligned network actually outperformed MWPM for all tested error rates up to the pseudo-threshold of around 0.12. (The pseudo-threshold is the noise parameter at which the logical error rate matches the error rate of two unencoded qubits.) Using $2.7 * 10^6$ data points, the uncentered network started to outperform MWPM, but only for error rates $p < 0.05$. Consistent improvements using uncentered data were only reached using $4.5 * 10^6$ training data points. This clearly shows that the size of the training set can be noticeably reduced when employing symmetries.

Similar effects could be observed on both the 3×3 and the 7×7 toric code. On the 3×3 code, the improvements gained by employing symmetries are much smaller. Here, a data set of size 10^6 was already sufficient to obtain large improvements over MWPM even without the use of symmetries. Two networks were trained, one with aligned data and one with uncentered data. Both networks used 2 hidden layers of sizes 500, 250, a training duration of 10^5 iterations and a constant learning rate of 0.001. The relative improvement of the aligned over the uncentered network at $p = 0.1$ was about 4%, and at $p = 0.03$ it was about 2%. Furthermore, it was noticeable that the training error of the aligned decoder was actually worse, while the validation error was improved. This is in contrast to the examples above, where both training and validation error were improved. Therefore it seems that in this case, the inclusion of symmetries mainly helps with generalization. In the examples on the 5×5 toric code above the



(a) Comparison of network error rates. The error rates of the decoders are compared relative to MWPM. Plotted is $p_{decoder}/p_{MWPM}$ for the different decoders. The dotted lines are only to guide the eye and do not represent actual data points. For $p \leq 0.05$, larger test sets of size 10^7 were used for increased accuracy. For $p = 0.01$ a test set of size $5 * 10^7$ was used in the aligned and centered case.



(b) Comparison of the network training.

Figure 5: Comparison of decoder on the 5×5 toric code using aligned, centered or uncentered training data. The training data sets had a size of $9 * 10^6$ and were generated at depolarizing noise parameter $p = 0.1$. The hyperparameters were the same for all networks:

layer sizes = 500, 250, $n_{it} = 100000$, $\eta = 0.001$

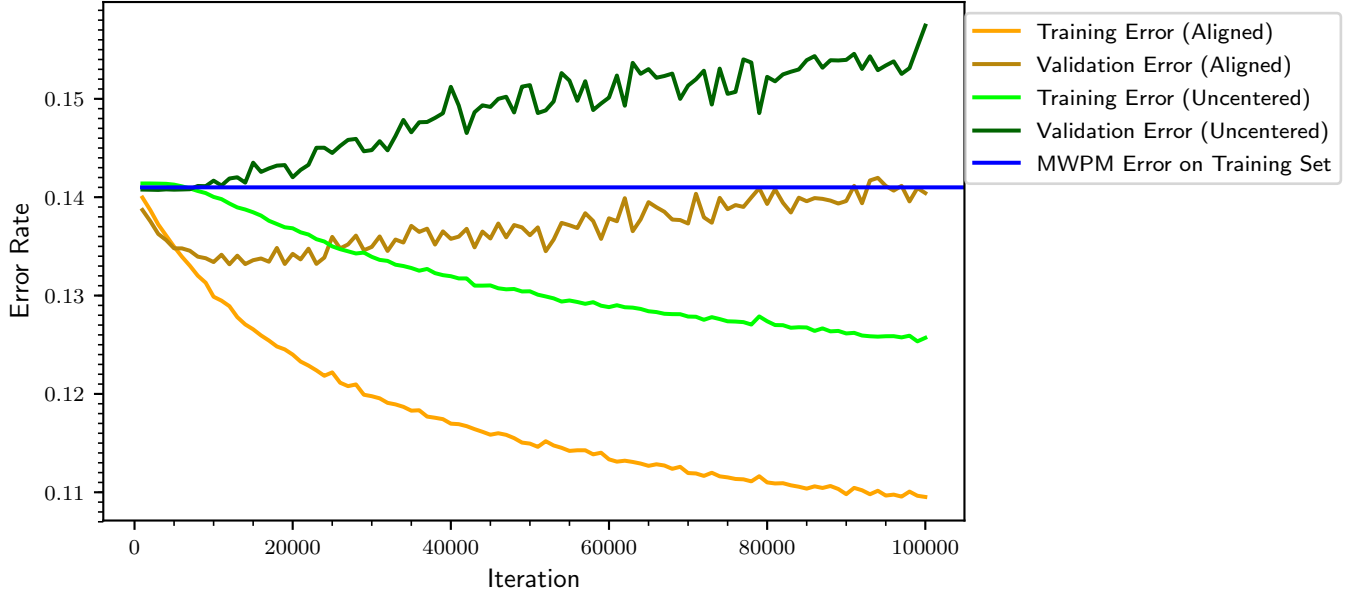


Figure 6: Comparison of network training on the 5×5 toric code with aligned or uncentered data sets of size 1.8×10^6 , generated at depolarizing noise parameter $p = 0.1$. The small training set size was chosen to test the minimum amount of training data that is needed to obtain improvements in the logical error rate.

Network parameters: layer sizes = 500, 250, $n_{it} = 100000$, $\eta = 0.001$

symmetries were also useful in finding a good fit to the training data at all. The main reason why the explicit inclusion of symmetries is less important for the 3×3 code is that the training set is large enough to learn the invariances by "brute force". For the 3×3 toric code, there are $2^{18} = 262144$ different syndromes, so one expects a large fraction of the possible syndrome to appear in a training set of size 10^6 . However for the 5×5 toric code there are $2^{50} \approx 1.1 \times 10^{15}$ different syndromes, so even a training set of size 10^7 will never cover the whole syndrome space. Therefore, for the 5×5 code, it is more important to introduce the invariances.

On the 7×7 code decoders were trained using up to 5×10^7 training examples. Without the use of symmetries, it was not possible to reach any improvements over MWPM. However, by aligning the training data, some improvements could be reached. It was possible to slightly outperform normal MWPM at all tested error rates. (Figure 7) The relative improvement was larger for smaller error rates. At large error rates the performance of the decoder was very close to MWPM.

As mentioned above, it is also possible to train an HLD on top of a trivial decoder instead of MWPM. This has the advantage that the decoding will be faster, and also training data can be generated faster. Therefore, it was also tested how symmetries affect the performance of an HLD when using the trivial decoder explained in section 3 as the underlying decoder. The trivial decoder itself has very bad error rates, worse

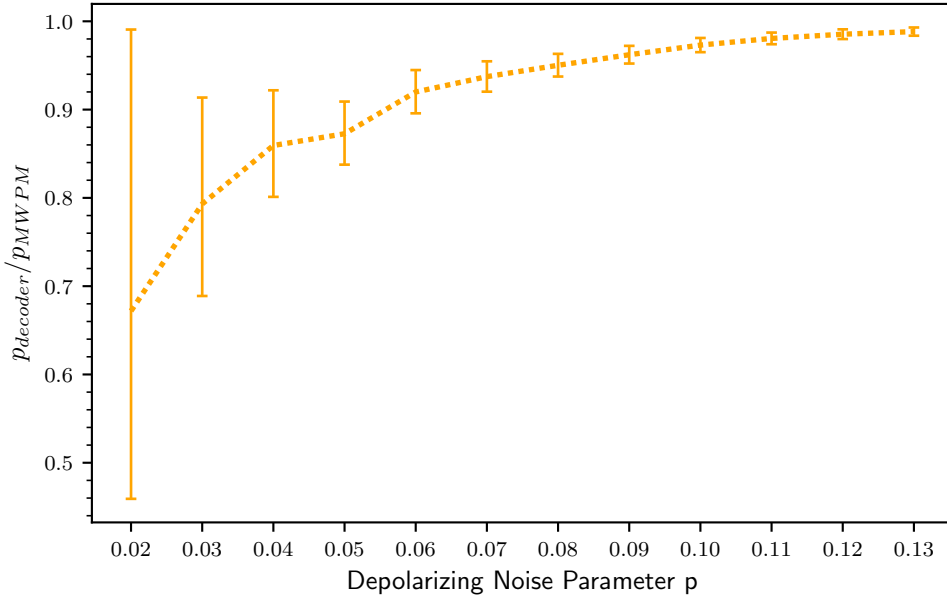


Figure 7: Performance of a high level decoder on the 7×7 toric code using an aligned training data set of size $4.5 * 10^7$ generated at depolarizing noise parameter $p = 0.1$. Shown is the relative improvement over MWPM. $p = 0.01$ is not plotted as both the decoder and MWPM performed perfectly on the test set. The large error bars at low p are due to the very low number of logical errors made by both MWPM and the HLD.

Network parameters: layer sizes = 500, 250, $n_{it} = 10^6$, $\eta = 0.001$

than those of two unencoded qubits. However the high level decoders based on it still produce good results. From here on we refer to high level decoders based on the trivial decoder as HLDT , and to high level decoders based on MWPM as HLDM . Two HLDTs were trained on the 5×5 toric code based on the same 10^7 physical errors also used above for Figure 5a. For one decoder the data was aligned, and the other used uncentered data. These two decoders were compared to the two HLDMs presented in Figure 5a. The same hyperparameters were used for training, with the exception of the training duration, which was longer for the HLDTs. Longer training was necessary for the error rates to converge. The HLDTs were trained for 10^6 iterations as opposed to 10^5 iterations for the HLDMs. The comparison of the logical error rates is shown in Figure 8. The logical error rates are again given relative to standard MWPM. It can be seen that the HLDTs perform worse than the corresponding HLDMs. However, the difference is noticeably smaller when employing symmetries. Furthermore, without symmetries, the HLDT outperforms MWPM only for small depolarizing noise parameters below 0.05, while for larger noise parameters it performs worse than MWPM. The performance of the HLDT is noticeably improved by the introduction of symmetries. It outperforms

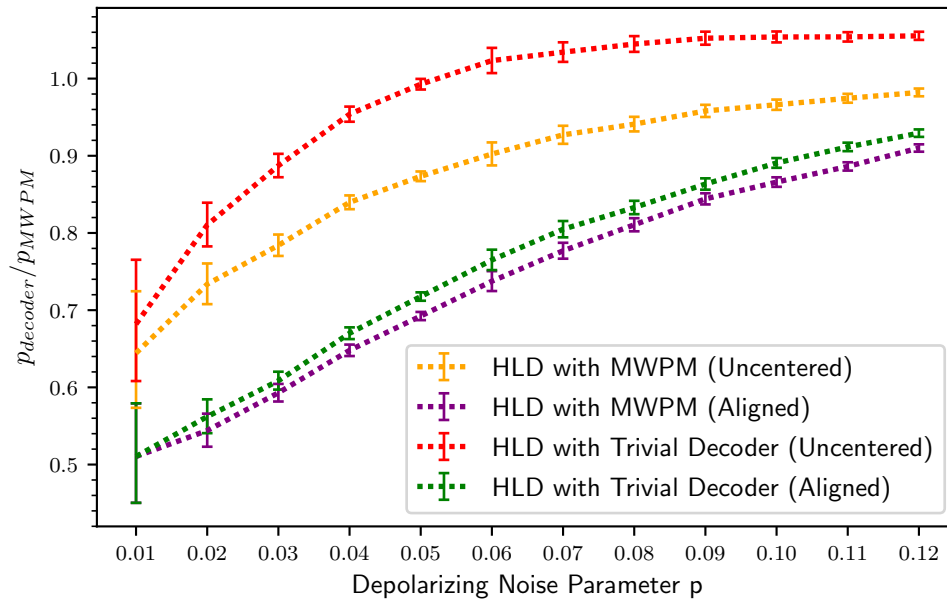


Figure 8: Comparison of different high level decoders on the 5×5 toric code relative to MWPM. Shown are high level decoders based on MWPM and high level decoders based on a trivial underlying decoder. In both cases both aligned and uncentered training sets of size 9×10^6 were used. For $p \leq 0.05$ larger test sets of size 10^7 were used for increased accuracy.

MWPM at all noise parameters. In fact, the aligned HLDT performs better than the uncentered HLDM. In conclusion, it is possible to use a fast but inaccurate underlying decoder to speed up the decoding process. The inclusion of symmetries is especially important in this case to minimize the decrease in accuracy.

7. Conclusion

The main result of this paper is that the performance of neural network based decoders for surface codes can be significantly improved by taking into account the symmetries of the code. A pre-processing algorithm with manageable overhead was proposed. This method was tested numerically for the high level neural network based decoder described in [21]. Tests were done for lattice lengths $L = 3, 5$ and 7 . Significant improvements were observed when accounting for symmetries. This allows for a reduced amount of training data, addressing one of the main problems pointed out in [4]. It is therefore one step in the direction of scalable neural network based decoders, although it does not seem sufficient by itself. In previous work [4, 21, 22] on high level decoders, the underlying decoder was always chosen to be fast but inaccurate. Here, it was experimentally demonstrated that an accurate underlying decoder also leads to a more accurate high level decoder in practice, i.e. not assuming perfect training. However, it was also shown that an

inaccurate underlying decoder can still lead to good results if the training is good enough. Therefore, the improvements reached by including symmetries were especially important in the case of a fast underlying decoder, which is also the most interesting case in practice. Additionally, it was shown that neural network based decoders can be applied to surface codes encoding more than one qubit. Although the inclusion of symmetries was demonstrated here for high level decoders, the core ideas and the pre-processing algorithm can likely be applied to other decoders.

For further research, it would be interesting to test these methods also for low level decoders (e.g. [20]). Furthermore, as mentioned above, the use of symmetries alone does not seem sufficient to allow for scalable neural network based decoders. Therefore it would be interesting to combine this approach with decoders based on local decompositions of the code (e.g. [18] and [23]).

Acknowledgments

We thank Kai Meinerz for interesting discussions about surface code decoding with neural networks. This project was funded by the Deutsche Forschungsgemeinschaft (DFG, German Research Foundation) under Germany's Excellence Strategy – Cluster of Excellence Matter and Light for Quantum Computing (ML4Q) EXC 2004/1 – 390534769 / Gefördert durch die Deutsche Forschungsgemeinschaft (DFG) im Rahmen der Exzellenzstrategie des Bundes und der Länder – Exzellenzcluster Materie und Licht für Quanteninformation (ML4Q) EXC 2004/1 – 390534769

References

- [1] D. Aharonov and M. Ben-Or. Fault Tolerant Quantum Computation with Constant Error. *arXiv e-prints*, art. quant-ph/9611025, Nov 1996.
- [2] S. Bravyi, M. Suchara, and A. Vargo. Efficient algorithms for maximum likelihood decoding in the surface code. *Phys. Rev. A*, 90:032326, 9 2014. doi: 10.1103/PhysRevA.90.032326. URL <https://link.aps.org/doi/10.1103/PhysRevA.90.032326>.
- [3] S. B. Bravyi and A. Y. Kitaev. Quantum codes on a lattice with boundary, 11 1998.
- [4] C. Chamberland and P. Ronagh. Deep neural decoders for near term fault-tolerant experiments. *Quantum Science and Technology*, 3(4):044002, 7 2018. doi: 10.1088/2058-9565/aad1f7. URL <https://doi.org/10.1088%2F2058-9565%2Faad1f7>.
- [5] L. DiCarlo, J. M. Chow, J. M. Gambetta, L. S. Bishop, B. R. Johnson, D. I. Schuster, J. Majer, A. Blais, L. Frunzio, S. M. Girvin, and R. J. Schoelkopf. Demonstration of two-qubit algorithms with a superconducting quantum processor. *Nature*, 460:240, 6 2009. URL <https://doi.org/10.1038/nature08121>.
- [6] G. Duclos-Cianci and D. Poulin. Fast decoders for topological quantum codes. *Phys. Rev. Lett.*, 104:050504, 2 2010. doi: 10.1103/PhysRevLett.104.050504. URL <https://link.aps.org/doi/10.1103/PhysRevLett.104.050504>.
- [7] J. Edmonds. Paths, trees, and flowers. *Canadian Journal of Mathematics*, 17: 449–467, 1965. doi: 10.4153/CJM-1965-045-4.
- [8] A. G. Fowler, M. Mariantoni, J. M. Martinis, and A. N. Cleland. Surface codes: Towards practical large-scale quantum computation. *Phys. Rev. A*, 86:032324, 9 2012. doi: 10.1103/PhysRevA.86.032324. URL <https://link.aps.org/doi/10.1103/PhysRevA.86.032324>.
- [9] I. Goodfellow, Y. Bengio, and A. Courville. *Deep Learning*. The MIT Press, 2016. ISBN 0262035618, 9780262035613.
- [10] A. A. Hagberg, D. A. Schult, and P. J. Swart. Exploring network structure, dynamics, and function using networkx. In G. Varoquaux, T. Vaught, and J. Millman, editors, *Proceedings of the 7th Python in Science Conference*, pages 11 – 15, Pasadena, CA USA, 2008.
- [11] A. Hutter, J. R. Wootton, and D. Loss. Efficient markov chain monte carlo algorithm for the surface code. *Phys. Rev. A*, 89:022326, 2 2014. doi: 10.1103/PhysRevA.89.022326. URL <https://link.aps.org/doi/10.1103/PhysRevA.89.022326>.
- [12] C. Igel, V. Heidrich-Meisner, and T. Glasmachers. Shark. *Journal of Machine Learning Research*, 9:993–996, 2008.
- [13] D. Katz, J. Baptista, S. P. Azen, and M. C. Pike. Obtaining confidence intervals for the risk ratio in cohort studies. *Biometrics*, 34(3):469–474, 1978. ISSN 0006341X, 15410420. URL <http://www.jstor.org/stable/2530610>.

- [14] D. P. Kingma and J. Ba. Adam: A method for stochastic optimization. In *3rd International Conference on Learning Representations, ICLR 2015, San Diego, CA, USA, May 7-9, 2015, Conference Track Proceedings*, 2015. URL <http://arxiv.org/abs/1412.6980>.
- [15] A. Y. Kitaev. Fault-tolerant quantum computation by anyons. *Annals of Physics*, 303(1):2 – 30, 2003. ISSN 0003-4916. doi: [https://doi.org/10.1016/S0003-4916\(02\)00018-0](https://doi.org/10.1016/S0003-4916(02)00018-0). URL <http://www.sciencedirect.com/science/article/pii/S0003491602000180>.
- [16] E. Knill, R. Laflamme, and W. Zurek. Threshold Accuracy for Quantum Computation, 10 1996.
- [17] N. Maskara, A. Kubica, and T. Jochym-O’Connor. Advantages of versatile neural-network decoding for topological codes. *Phys. Rev. A*, 99:052351, May 2019. doi: 10.1103/PhysRevA.99.052351. URL <https://link.aps.org/doi/10.1103/PhysRevA.99.052351>.
- [18] X. Ni. Neural Network Decoders for Large-Distance 2D Toric Codes. *arXiv e-prints*, art. arXiv:1809.06640, Sep 2018.
- [19] R. Raussendorf and J. Harrington. Fault-tolerant quantum computation with high threshold in two dimensions. *Phys. Rev. Lett.*, 98:190504, 5 2007. doi: 10.1103/PhysRevLett.98.190504. URL <https://link.aps.org/doi/10.1103/PhysRevLett.98.190504>.
- [20] G. Torlai and R. G. Melko. Neural decoder for topological codes. *Phys. Rev. Lett.*, 119:030501, 7 2017. doi: 10.1103/PhysRevLett.119.030501. URL <https://link.aps.org/doi/10.1103/PhysRevLett.119.030501>.
- [21] S. Varsamopoulos, B. Criger, and K. Bertels. Decoding small surface codes with feedforward neural networks. *Quantum Science and Technology*, 3(1):015004, 11 2017. doi: 10.1088/2058-9565/aa955a. URL <https://doi.org/10.1088/2F2058-9565%2Faa955a>.
- [22] S. Varsamopoulos, K. Bertels, and C. G. Almudever. Designing neural network based decoders for surface codes. arXiv:1811.12456, 2018.
- [23] S. Varsamopoulos, K. Bertels, and C. G. Almudever. Decoding surface code with a distributed neural network based decoder. *arXiv e-prints*, art. arXiv:1901.10847, Jan 2019.